ASTRONOMY & ASTROPHYSICS
SUPPLEMENT SERIES

Astron. Astrophys. Suppl. Ser. **126,** 393-400 (1997)

ESO & NOT photometric monitoring of the Cloverleaf quasar⋆,⋆⋆

R. Østensen[1], M. Remy[2], P.O. Lindblad[3], S. Refsdal[4], R. Stabell[5], J. Surdej[2,⋆⋆⋆], P.D. Barthel[6], P.I. Emanuelsen[1], L. Festin[7], E. Gosset[2,†], O. Hainaut[8], P. Hakala[9], M. Hjelm[3], J. Hjorth[10], D. Hutsemékers[2,⋆⋆⋆], M. Jablonski[5], A.A. Kaas[3], H. Kristen[3], S. Larsson[3], P. Magain[2‡], B. Pettersson[7], A. Pospieszalska-Surdej[2], A. Smette[6], J. Teuber[11], B. Thomsen[12], and E. Van Drom[2]

[1] Institute of Mathematical and Physical Sciences, University of Tromsø, N-9037 Tromsø, Norway
[2] Institut d'Astrophysique, Université de Liège, Belgium
[3] Stockholm Observatory, S-13336 Saltsjöbaden, Sweden
[4] Hamburger Sternwarte, Gojenbergsweg 112, D-21029, Germany
[5] Institute of Theoretical Astrophysics, University of Oslo, Box 1029 Blindern, N-0315 Oslo, Norway
[6] Kapteyn Astronomical Institute, Rijksuniversiteit, Landleven 12, Postbus 800, 9700 AV Groningen, The Netherlands
[7] Astron. Obs. Box 515, S-751 20 Uppsala, Sweden
[8] Institute for Astronomy, 2680 Woodlawn Drive, Honolulu HI 96822, U.S.A.
[9] Helsinki University Observatory, Tahtitorninmaki, SF-00014 Helsinki, Finland
[10] NORDITA, Blegdamsvej 17, DK-2100 Copenhagen, Denmark
[11] Copenhagen University Observatory, Juliane Maries Vej 30, DK-2100 Copenhagen, Denmark
[12] Institute of Physics and Astronomy, University of Aarhus, DK-8000 Aarhus C, Denmark

Received November 18, 1996; accepted March 18, 1997

Abstract. The Cloverleaf quasar, H1413+117, has been photometrically monitored at ESO (La Silla, Chile) and with the NOT (La Palma, Spain) during the period 1987–1994. All good quality CCD frames have been successfully analysed using two independent methods (i.e. an automatic image decomposition technique and an interactive CLEAN algorithm). The photometric results from the two methods are found to be very similar, and they show that the four lensed QSO images vary significantly in brightness (by up to 0.45 mag), nearly in parallel. The lightcurve of the D component presents some slight departures from the general trend which are very likely caused by micro-lensing effects. Upper limits, at the 99% confidence level, of 150 days on the absolute value for the time delays between the photometric lightcurves of this quadruply imaged variable QSO, are derived. This is unfortunately too large to constrain the lens model but there is little doubt that a better sampling of the lightcurves should allow to accurately derive these time delays. Pending a direct detection of the lensing galaxy (position and redshift), this system thus constitutes another good candidate for a direct and independent determination of the Hubble parameter.

Key words: gravitational lensing — techniques: image processing — quasars: H1413+117

1. Introduction

The Cloverleaf quasar, H1413+117, was discovered to be a quadruply imaged QSO by Magain et al. (1988). Since then, it has been photometrically monitored essentially as part of the ESO Key-Program *Gravitational Lensing* (La Silla) and as part of the *Gravitational Lens Monitoring Program* at the Nordic Optical Telescope (NOT) on the island of La Palma. This quasar, at a redshift of 2.55, and with an apparent visual magnitude of 17, is one of the brightest members of the class of broad absorption line (BAL) QSOs. In addition, its spectrum shows at least three narrow absorption line systems at redshifts $z = 1.44$, 1.66 and 2.07. These are attributed to intervening gas

Send offprint requests to: rolf.stabell@astro.uio.no

⋆ Based on observations collected at the European Southern Observatory (La Silla, Chile) and with the Nordic Optical Telescope (La Palma, Spain).

⋆⋆ Table 1. Logbook for the ESO and NOT observations together with photometric results for the Cloverleaf quasar. This long table can be accessed on the WWW at the URL address: http://vela.astro.ulg.ac.be/grav_lens/glp_homepage.html

⋆⋆⋆ Research Director, Belgian Fund for Scientific Research (FNRS).

† Research Associate, Belgian Fund for Scientific Research (FNRS).

‡ Senior Research Associate, Belgian Fund for Scientific Research (FNRS).

clouds (Hazard et al. 1984; Drew & Boksenberg 1984; Turnshek et al. 1988), possibly associated with the lens(es) (Magain et al. 1988). Imaging of H1413+117 shows that the four lensed components are separated by approximately one arcsecond ($''$). However, no lensing object has yet been detected. The spectra of two of the four images have been found by Magain et al. (1988) to be identical, except for narrow absorption line systems at $z = 1.44$ and 1.66, which are much stronger in component B than in C. Two-dimensional spectroscopy by Angonin et al. (1990) also shows that the spectrum of component D has smaller values for the emission lines/continuum ratios and a larger equivalent width for the absorption features in the P Cygni profiles, compared to the other three lensed QSO components. This is most likely caused by micro-lensing effects. Observations from the VLA at NRAO show radio counterparts for the four QSO components, as well as an additional strong radio source between images B and D (Kayser et al. 1990), but no radio source has been found that can be associated with a lensing object.

As part of the *Gravitational Lensing* ESO Key-Program, CCD photometry of H1413+117 has been carried out with the aim of detecting photometric variability of the QSO itself, and thereby determining the time delay(s), or the signature of micro-lensing effects. Preliminary results for the four images have been presented by Arnould et al. (1993) and by Remy et al. (1996). These authors report that from 1987 to 1993 the four lensed components apparently display brightness variations quasi-simultaneously and in parallel. They set an upper limit for the time delays of roughly a few months. In addition to these variations, which are ascribed to the source, the D component has been found to show extra light variations with respect to the other components. These extra variations have been interpreted as being possibly induced by micro-lensing effects.

The astrophysical and cosmological justifications for conducting photometric monitoring programs of gravitational lens systems are summarized in Refsdal & Surdej (1992, 1994). The importance of recording well sampled and accurate lightcurves for such systems can hardly be overestimated. The ESO Key-Program observations took place during the period 1987-1993 (see Table 1, accessible on the WWW).

The original plans were to monitor the known gravitational lens systems Q2237+0305 (the Einstein Cross), UM425, Q0142 − 100 = UM673 (ESO GL1, Surdej et al. 1987, 1988) and H1413+117 (the Cloverleaf), at weekly intervals. However, because of unfavorable weather conditions, unexpected technical problems or sometimes the non-availability of a direct CCD camera at the foci of the ESO telescopes, the sampling of the photometric lightcurves has not been as frequent as initially expected. After some preliminary observations in 1990, a program was also started at the NOT, for monitoring the four gravitational lens systems Q0142 − 100, Q0957+561 (the "classical" Double Quasar), H1413+117 and Q2237+0305. Although observations were similarly aimed at weekly intervals, several large gaps in the NOT data have occurred for the same reasons as those mentioned above. Results for the Einstein Cross have been published by Østensen et al. (1996), for UM425 by Courbin et al. (1995) and for Q0142 − 100 by Hjorth et al. (1996) and Daulie et al. (1993).

In this paper we present results for the Cloverleaf, obtained using two independent methods of analysis, combining all ESO and NOT observations.

2. Observations and instrumentation

The ESO Key-Program observations of the Cloverleaf were made using several different telescopes, and with a number of different CCD detectors. All telescopes and cameras used are listed in Table 1, together with the filters, observing dates, average seeing and the name of the principal investigator(s). The ESO telescopes that were used are the 3.5 m New Technology Telescope (NTT), the 2.2 m ESO-Max Planck Institut (MPI) telescope and the Danish 1.54 m telescope (DAN) at La Silla, Chile (the ESO 3.6 m telescope has also been used occasionally).

Observations from the NOT Monitoring program were made with the 2.56 m Nordic Optical Telescope, at Roque de los Muchachos, La Palma, Canary Islands (Spain) from April 1990 to August 1994. During the first four years, a Tektronix 512 × 512 CCD camera with 0.197$''$ pixels was the only detector available. In 1994, a more sensitive 1024 × 1024 CCD camera with 0.177$''$ pixels was installed. Reasonable signal-to-noise ratios were obtained for exposure times of 4 minutes or more when the seeing was better than 1$''$. The best NOT images show point source profiles with $FWHM = 0.5''$, which clearly resolve the four optical components of the Cloverleaf. Note that a non-linearity problem with the NOT stand-by CCD camera in observations made before 1993 has been numerically corrected for (see Østensen et al. 1996).

3. Data reduction, calibration and image analysis

Two independent methods have been used to preprocess and analyse all CCD frames obtained for the Cloverleaf at ESO and with the NOT. These are described below.

3.1. Automatic image decomposition technique

Classical preprocessing (flat-field correction and bias subtraction) has been applied to the raw data using ESO MIDAS routines. Whenever necessary, CCD non-linearities have been corrected for. Other defects such as column offsets and cosmic rays have been removed before sky subtraction. On each image frame, bi-quadratic polynomial surfaces have been fitted to numerous selected empty regions of the observed fields, in order to accurately subtract the sky from each individual CCD frame.

Also in the MIDAS environment, a general, automatic procedure has been developed in order to derive the best photometric measurements of multiply imaged point sources. The magnitudes of the lensed components have been determined by fitting multiple numerical point spread functions (hereafter PSFs), using a χ^2 minimization method.

The numerical PSF has been determined by summation of the images of isolated point sources recorded on the same CCD frames as the gravitational lens system, after re-centering at the same position by bi-quadratic interpolations. Figure 1 in Kayser et al. (1990) shows a finding chart around H1413+117, with several of the used PSF stars. Star 40 has been adopted as our photometric reference. Among others, stars 8, 19, 40, 45 and 47 have frequently been used to construct the PSF. After fitting the composite PSF to the individual stars present on the CCD frame, incompatible objects were removed and the PSF redetermined. Making use of the coordinates of the stars derived from the previous fits, the linear transformation of the positions between different frames could be determined very accurately, including any relative rotation, translation and scaling.

On each individual frame, four free PSFs were first fitted to the complex QSO image, leading to positions for each of the four lensed components and preliminary values for the intensities. In Fig. 1 the relative positions of the four lensed images of the QSO are plotted. In the final measurements, the relative positions of the four PSFs have been fixed, reducing the number of free parameters from 12 to 6 (i.e. 4 intensity parameters and 2 position parameters). The values of these average relative image positions are shown in Table 2; the estimated uncertainties being $\sigma \simeq 0.008''$. A complete description of this automatic decomposition technique may be found in Remy (1996). Let us finally note that a total of 157 distinct ESO and NOT observations have been successfully analysed with the above method, even the lower quality data.

Table 2. Average relative positions of the B, C and D lensed components with respect to A, as derived from the multiple fitting of 4 free PSFs applied to a set of the 80 best ESO and NOT observations

Comp.	$\Delta\alpha$ ($''$)	$\Delta\delta$ ($''$)
A	+0.000	+0.000
B	+0.726	+0.201
C	−0.518	+0.705
D	+0.324	+1.058

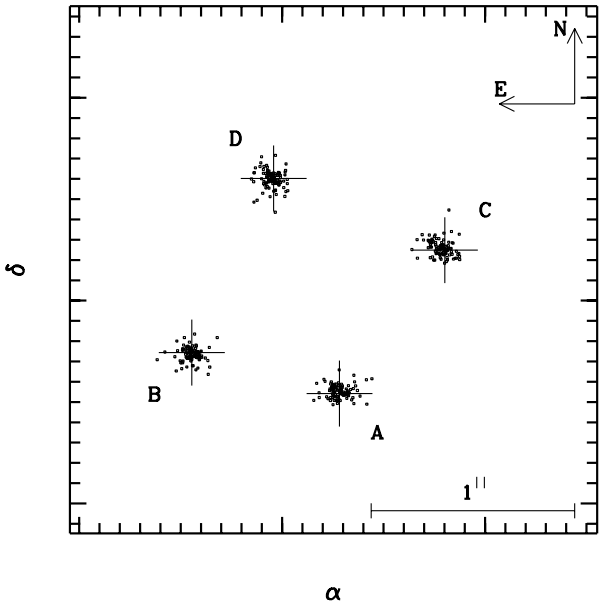

Fig. 1. Relative positions of the four lensed components of H1413+117 derived from multiple PSF fittings of the 80 best ESO and NOT observations. The four crosses in this figure refer to the adopted average relative positions of the four lensed QSO images used in subsequent PSF fittings (see Table 2)

3.2. Interactive CLEAN processing

We have independently applied the IRAF/ccdred package developed and maintained by NOAO (National Optical Astronomy Observatories, Tucson, Arizona) to preprocess the same ESO and NOT data.

A program for CLEAN deconvolution of overlapping point sources has been developed by Østensen (1994), and implemented using IDL. This program, XECClean, was especially developed for doing high precision photometry of the quadruply imaged system, Q2237+0305 (the Einstein Cross). XECClean applies a semi-analytical PSF-profile fitting procedure adopted from the DAOPHOT package by Stetson (1987) and deconvolves the images using the interactive CLEAN algorithm (Teuber 1993), where the individual images are iteratively removed, until satisfactory residuals are obtained. Unlike for the case of the Einstein Cross, the analysis of the Cloverleaf system does not suffer from the additional presence of a bright foreground lens, and it is therefore easier to determine the individual fluxes of the four QSO components.

For some of the ESO data, photometric standard stars have been simultaneously observed in the V and R bands. From this, we have calibrated in magnitude several of the used PSF stars. Adopting the numbering used by Kayser et al. (1990) for the identification of the comparison stars, we report in Table 3 their V and R magnitudes. The photometric variability of star 40 has been checked against star 45. These stars are found to be photometrically

stable with respect to each other and to other PSF stars. Since star 40 is present on all CCD frames obtained for H1413+117, it has been used as our photometric reference star.

Table 3. V and R magnitudes of PSF stars in the field of H1413+117. See Kayser et al. (1990) for a finding chart. The 1σ uncertainty on the zero point magnitude determinations is about 0.10 mag

Star	V	R
40	18.55	17.89
8	18.72	18.41
19	18.09	17.38
45	16.88	16.41
47	20.32	19.56

4. Photometric results

The relative magnitudes of the four lensed components of the Cloverleaf determined with respect to the photometric reference star 40 are also reported in Table 1. Furthermore, this table lists details of the observations together with the Modified Julian Day at the time of the observations, night averages of the photometric determinations derived from applying the automatic image decomposition technique (i.e. A_1, B_1, C_1, D_1 for the relative photometric measurements of the A-D components, respectively, and $\sigma_1(A)$, $\sigma_1(B)$, $\sigma_1(C)$, $\sigma_1(D)$, for the derived measurement uncertainties as described below) and from applying the interactive CLEAN algorithm (i.e. A_2, B_2, C_2, D_2 and σ_2 for a common value of the measurement uncertainties). The same photometric measurements with their uncertainties are plotted in Fig. 2 (automatic image decomposition technique, method 1) and in Fig. 3 (interactive CLEAN processing, method 2), as a function of the Modified Julian Day.

We describe in this paragraph how the photometric error bar with the automatic image decomposition technique has been derived for a given science frame. A simulated frame which mimics the science frame has been constructed. Gaussian profiles with comparable intensities, relative image positions and FWHM were used to simulate the real objects. Random values have been added to the simulation in a coherent way with the noise characteristics of the real frames. The simulated frame has then been reduced in exactly the same way as the real observations (including PSF determination with the same stars). This (very time consuming) simulation process has been repeated 10 times with different random noise values (still in a coherent way with the noise in the real frame). The dispersions of the derived values for each simulation of the set lead to realistic estimates for the photometric error bars (i.e. $\sigma_1(A)$, $\sigma_1(B)$, $\sigma_1(C)$, $\sigma_1(D)$). Such estimates have also been compared with the dispersion of measurements made on a series of 15 real observations, taken during the same night in the Gunn i filter (for which we assume intra-night photometric constancy): a good agreement has been found. Despite the fact that the error estimates for the automatic method are the best ones available, we cannot rule out an underestimation of the error (maximum by a factor 2) for some of the photometric data, especially those with a seeing > 1.4.

When using the interactive CLEAN algorithm, the error estimates are based on both the statistical uncertainties, as derived from the XECClean fitting, and the residuals in the CLEAN'ed image. The latter contribution includes the effects from seeing conditions and the quality of the PSF. Zero-point errors occurring when using a calibration star in the field, with colors different from the program object, can be as large as 0.02 magnitudes when changing from one detector to another.

Since our observations have been made using such a wide range of telescopes and CCD cameras, and since it has not been possible to maintain exactly the same set of filters throughout the monitoring period, some additional uncertainties are introduced in our data. However, all estimates show that these errors should be small compared to those due to the photometric decomposition of the four lensed QSO images.

5. Discussion

Comparison between the photometric lightcurves illustrated in Figs. 2 and 3 for the A, B, C and D lensed components of H1413+117 reveals a remarkably good match between the measurements derived using the two independent image analysis methods described in the previous section. Figure 4 compares the photometric measurements and their uncertainties derived using the two independent methods. Except for a few isolated data points, there is a very good overall agreement between these independent photometric determinations.

From our two observations in the B band (see Table 1), we note that the B component is weaker than the C component, while being almost equal in the V band (see Fig. 2 and Fig. 3). Image B is also markedly stronger than image C in the I band than in the R band (see Table 1 for the independent photometric measurements). This is consistent with differential reddening caused by dust in the lensing galaxy along the different light paths of the lensed components. The prominence of absorption lines at redshifts $z = 1.44$, 1.66 in the spectrum of component B supports this interpretation (Magain et al. 1988) and

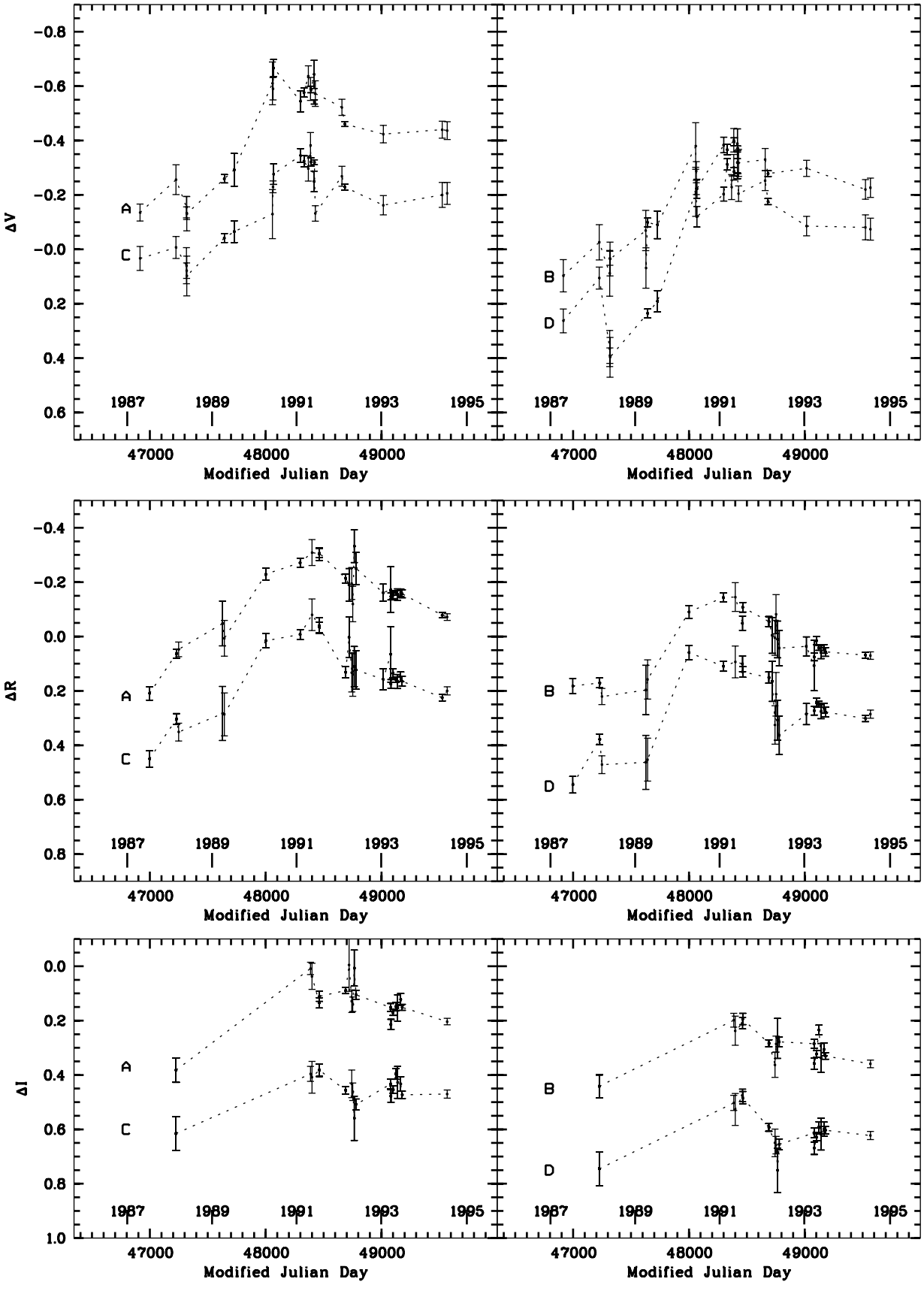

Fig. 2. Relative V, R and I magnitudes of the four lensed components of H1413+117 with respect to the photometric reference star as a function of the Modified Julian Day. These measurements are the results of applying the automatic image decomposition technique (see text, method 1)

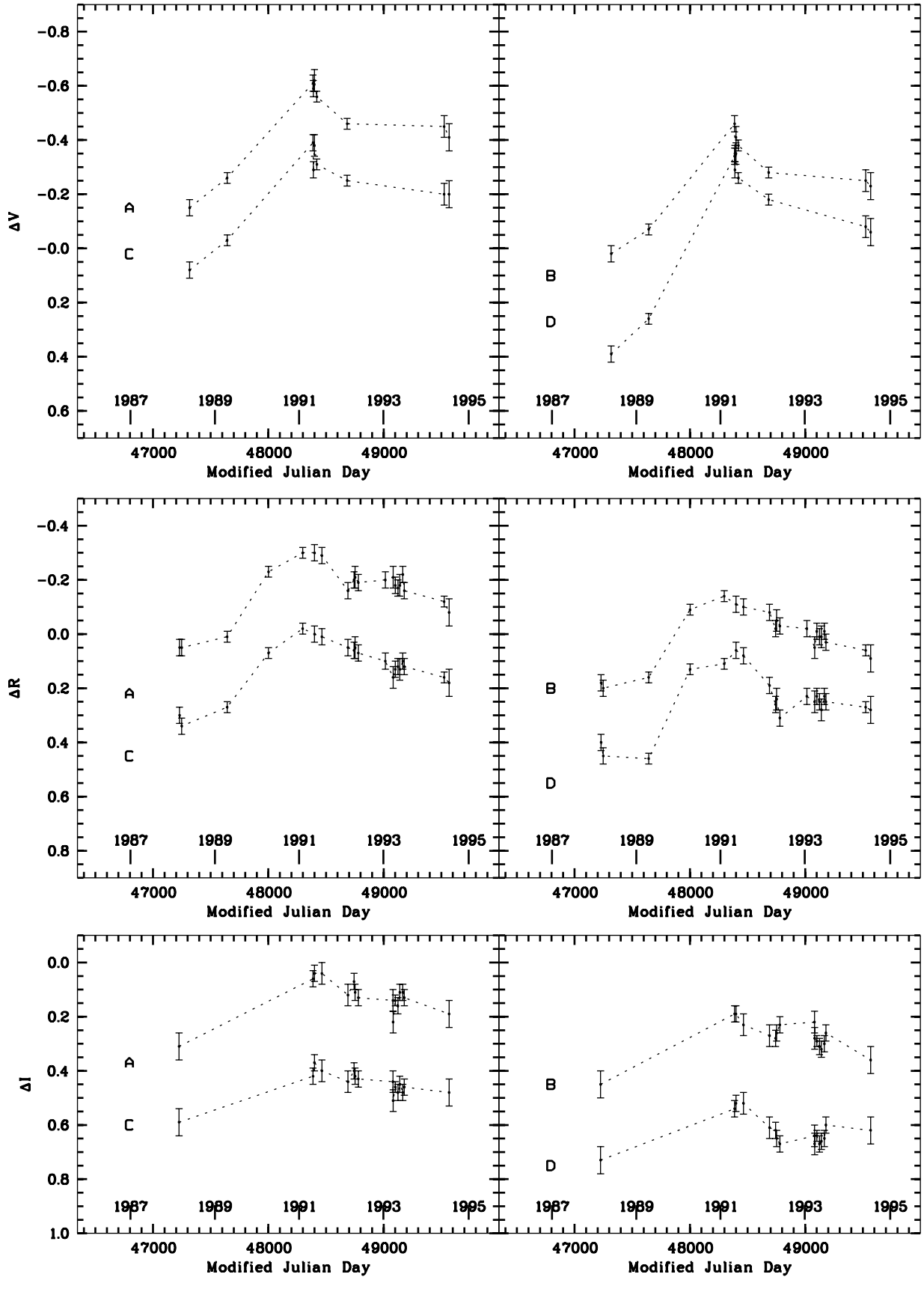

Fig. 3. Relative V, R and I magnitudes of the four lensed components of H1413+117 with respect to the photometric reference star as a function of the Modified Julian Day. These measurements are the results of applying the interactive CLEAN algorithm (see text, method 2)

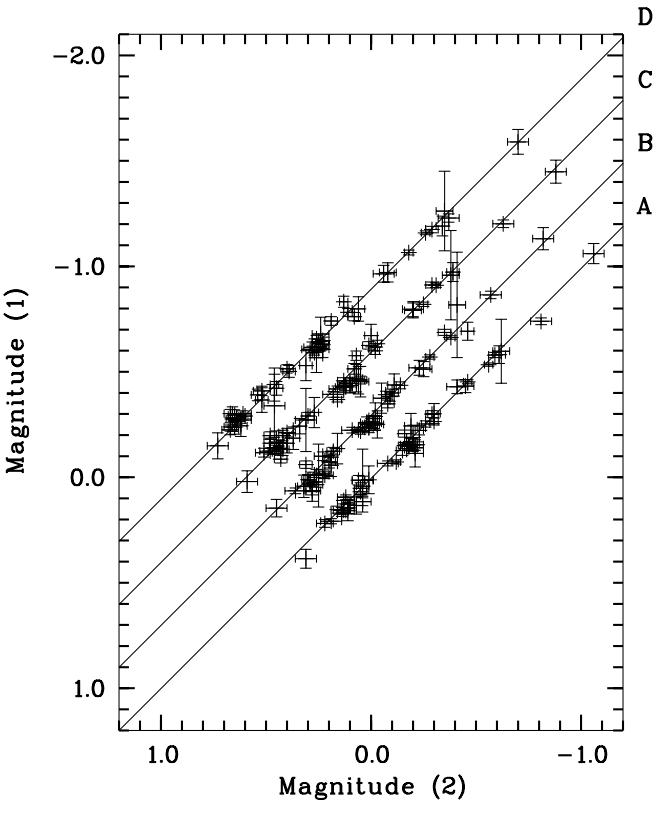

Fig. 4. Relative magnitudes for the A, B, C and D lensed components of H1413+117 (all filters), with respect to the reference photometric star, derived using the automatic image decomposition technique (1) and the interactive CLEAN algorithm (2). The diagonal lines represent curves of perfect match between the two methods. Note that for the sake of clarity, the measurements pertaining to B, C, D and their associated diagonal lines have been translated by constant values with respect to the results for A

suggests searching for the lensing object(s) at those redshifts, in the vicinity of the B component.

The lightcurves for the A, B and C components clearly vary in a parallel fashion in all filters, starting at a minimum luminosity in 1988, at the beginning of the ESO observation series, and peaking in 1991. The time delay for this system is expected to be shorter than one month (Kayser et al. 1990), so the quasi-simultaneous variations observed for these three components are consistent with intrinsic variations, as previously noted by Arnould et al. (1993) and Remy et al. (1996).

In order to avoid windowing effects on the time delay determinations (see Kayser 1993), the V and R lightcurves of component A, derived with method 1, have been smoothed using a simple low-pass spline with cut-off frequency of about (2 weeks)$^{-1}$. The magnitude differences between the data and the smoothed curve fall approximately within the 3σ limit. Nevertheless, the χ^2 for those magnitude differences, in a given filter, is found to be too high by a factor 4, at least. This could indicate the existence of photometric variations at higher frequencies but also of non-Gaussian errors or an oversmoothing of the data. In the next step of the analysis, the two smoothed lightcurves for component A (one for R and one for V) have been numerically translated in the epoch–magnitude diagram (Δt, Δm). For a given value of (Δt, Δm), the corresponding χ^2 between the observations of a given component and the point of the translated smoothed lightcurve at the same epoch has been computed. As the high frequency variations disallow a direct statistical interpretation of the χ^2 values, the latter ones have been normalized in two ways.

If we assume that the smoothed lightcurve of A should be compatible with the A data, the χ^2 for each component have been normalized to the minimum χ^2 of A (solid contours in Fig. 5). Considering the A data points, the derived $\chi^2(\Delta t, \Delta m)$ contour at the 99% confidence level (combined for the V and R filters in Fig. 5), extends to about $\pm$150 days. This sets a lower limit on the accuracy of the time delay determination based on this technique with the present data. For the B and C components, the time delays corresponding to a minimum χ^2 computed independently for the two filters (not represented) are found to be non-consistent. This accounts for the relatively smaller size of the 99% compatibility domain of the combined χ^2 for components B and C (see Fig. 5). No acceptable values for the χ^2 were found for the D component at the 99% confidence level. This is a definite indication for an abnormal behavior of the D lightcurve, incompatible with the simple interpretation in terms of time delay.

The χ^2 for each component has also been normalized to the local minimum of that component (dashed contours in Fig. 5). With this normalization, differences in the curves which would be incompatible with the hypothesis of the time delay phenomenon are hidden. An upper limit of about 150 days on the absolute value for the time delays remains. All the curves are thus also compatible with zero time delay.

We conclude that the present lightcurves of the Cloverleaf quasar are not sufficiently well sampled and/or accurate in order to estimate precise values for the time delays, only upper limits can be set. However, given the noticeable intrinsic photometric variability of H1413+117, we feel confident that a better sampling of the lightcurves will lead to an accurate determination of the time delays for this system.

Analysis of our observations does not show any clear sign of micro-lensing activity for the A, B and C components. The photometric variations for the D component, however, deviate somewhat from the parallel behavior seen for the other three lensed QSO images. Particularly during the 1992 season, there is a steep decrease in the flux of this component by approximately 0.1 magnitude during three months, while the other components remain

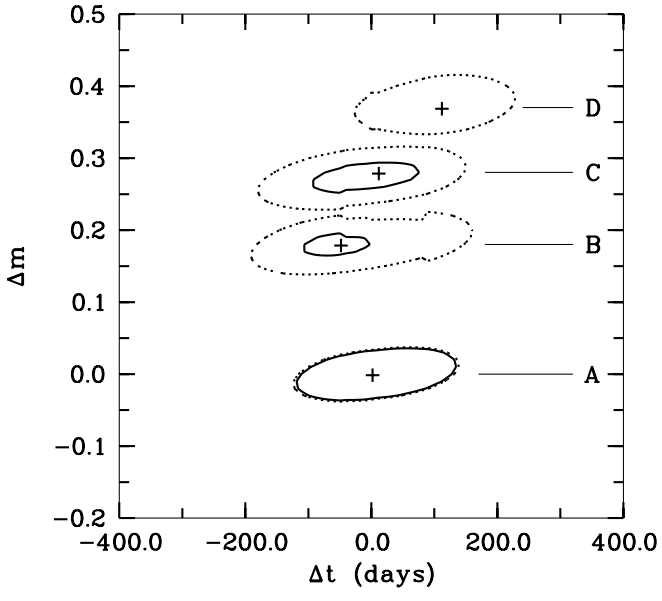

Fig. 5. 99% confidence level contours for the χ^2 of the differences between a smoothed lightcurve of component A, translated by Δt in epoch and Δm in magnitude, and the measurements of the four components, as derived by method 1. The smoothed lightcurve has been defined by a spline interpolation of the A measurements; hence the differences in epoch and magnitudes are relative to A. The χ^2 computed independently for the V and R data have been combined in the present diagram and normalized to the minimum χ^2 for A (solid contours) or to the minimum χ^2 for the given component (dashed contours). Crosses indicate the positions of the minima

relatively constant. The event is seen in both the I and R bands, whereas the V and B bands have insufficient observations to substantiate this. Variations during 1988 for the D component reported by Remy et al. (1996) in the V band were also interpreted as being possibly caused by micro-lensing. Angonin et al. concluded from spectra obtained on March 7, 1989 that the continuum of image D was slightly bluer than the other three images. From our observations in 1988 and 1994 we find no significant blue excess in the D component to within 0.03 mag. Unfortunately the observations from 1989 are not of sufficient quality to draw any definite conclusions.

In conclusion, pending a direct identification of the lensing galaxy, the multiply imaged QSO H1413+117 constitutes a very good candidate for a direct and independent determination of the Hubble parameter H_0. A photometric monitoring of this optical source, with optimal time coverage, should be organized in the near future. International collaboration will be essential for its success.

Acknowledgements. RØ would like to thank the STScI, the Norwegian Research Council and the Stockholm Observatory for financial support during a two month stay at STScI. MR and JS would like to thank B. Revenaz for his help at STScI and the PRODEX grant "Gravitational Lensing with HST" for financial support. AS thanks for financial support under grant no 781-73-058 from the Netherlands Foundation for Research in Astronomy (ASTRON) which receives its funds from the Netherlands Organisation for Scientific Research (NWO).

References

Angonin M.-C., Remy M., Surdej J., Vanderriest C., 1990, A&A 233, L5
Arnould P., Remy M., Gosset E., et al., 1993, Proc. 31st Liège Int. Astrophysical Coll. "Gravitational Lenses in the Universe", Surdej J. et al. (eds.), p. 169
Courbin F., Magain P., Remy M., et al., 1995, A&A 303, 1
Daulie G., Hainaut O., Hutsemékers D., et al., 1993, Proc. 31st Liège Int. Astrophysical Coll. "Gravitational Lenses in the Universe", Surdej J. et al. (eds.), p. 181
Drew J.E., Boksenberg A., 1984, MNRAS 211, 813
Hazard C., Morton D.C., Terlevich R., McMahon R., 1984, ApJ 282, 33
Hjorth J., Refsdal S., Stabell R., et al., 1996 (submitted to A&A)
Kayser R., Surdej J., Condon J.J., et al., 1990, ApJ 364, 15
Kayser R., 1993, Proc. 31st Liège Int. Astrophysical Coll. "Gravitational Lenses in the Universe", Surdej J. et al. (eds.), p. 5
Magain P., Surdej J., Swings J.-P., et al., 1988, Nat 334, 325
Østensen R., 1994, Cand. Scient. Thesis, University of Tromsø
Østensen R., Refsdal S., Stabell R., et al., 1996, A&A 309, 59
Refsdal S., Surdej J., 1992, Highlights Astron. 9, 3
Refsdal S., Surdej J., 1994, Rep. Prog. Phys. 56, 117
Remy M., Gosset E., Hutsemékers D., et al., 1996, IAU Symp. 173, "Astrophysical applications of Gravitational Lensing", Kochanek C.S. & Hewitt J.N. (eds.), p. 261
Remy M., 1996, Ph.D. Thesis, Liège University
Stetson P.B., 1987, PASP 99, 191
Surdej J., Magain P., Swings J.-P., et al., 1987, Nat 329, 695
Surdej J., Magain P., Swings J.-P., et al., 1988, A&A 198, 49
Teuber J., 1993, Digital Image Processing. Prentice-Hall
Turnshek D.A., Foltz C.B., Grillmair C.J., Weymann R.J., 1988, ApJ 325, 651